This is an open access article published under a Creative Commons Attribution (CC-BY) License, which permits unrestricted use, distribution and reproduction in any medium, provided the author and source are cited.

ACS AUTHORCHOICE

ACS OMEGA

Article

Cite This: ACS Omega 2020, 5, 1472−1478

Electronic Structure and Conformational Properties of Polybenzimidazole-Based Ionenes—A Density Functional Theory Investigation

Mehrdad Mokhtari,[†,§] Mohammad Javad Eslamibidgoli,[*,†,§] and Michael H. Eikerling[†,‡]

[†]Department of Chemistry, Simon Fraser University, 8888 University Drive, V5A 1S6 Burnaby, British Columbia, Canada

[‡]IEK-13, Institute of Energy and Climate Research, Forschungszentrum Jülich GmbH, 52425 Jülich, Germany

ABSTRACT: Polybenzimidazole-based ionenes are explored for use in both alkaline anion-exchange membrane fuel cells and alkaline polymer electrolyzers. Poly-(hexamethyl-*p*-terphenylbenzimidazolium) (HMT-PMBI), the material of interest in this article, is exceptionally hydroxide-stable and water-insoluble. The impact of the degree of methylation on conformations and electronic structure properties of HMT-PMBI oligomers, from the monomer to the pentamer, is studied with density functional theory calculations. Optimization studies are presented for both the gas phase and in the presence of implicit water. In addition, time-dependent density functional theory is employed to generate the UV−vis absorption spectra of the studied systems. Results are insightful for experimentalists and theorists investigating the impact of synthetic and environmental conditions on the conformation and electronic properties of polybenzimidazole-based membranes.

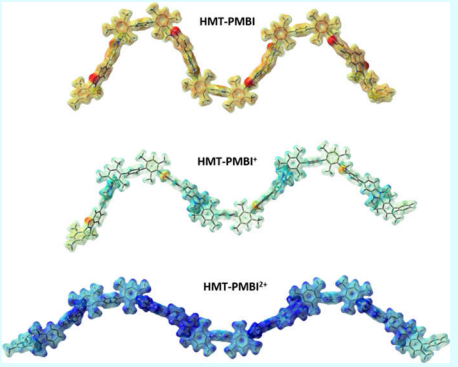

Downloaded via FORSCHUNGZENTRUM JUELICH on October 16, 2020 at 14:28:13 (UTC).
See https://pubs.acs.org/sharingguidelines for options on how to legitimately share published articles.

1. INTRODUCTION

Research on anion-exchange membranes (AEMs) is thriving, propelled by their promising potential for uses in alkaline electrochemical energy technologies such as fuel cells,[1−3] water electrolyzers,[4] redox flow batteries,[5] and waste-water treatment systems.[6] Alkaline conditions offer distinct advantages over acidic conditions. A major driver for the development of alkaline technologies is the possible replacement of Pt- by Ni-based materials as oxygen reduction catalysts.[7] AEMs that are already being tested in fuel cells possess relatively simple synthetic routes, which is another advantage over proton-conducting polymer electrolyte membranes (PEMs).[2,8] AEMs also show promise in reducing the membrane sensitivity to variations in the hydration level, which could reduce humidification requirements and electrode flooding, and thereby diminish system costs.[7,9]

On the flip side, a decade ago, the ion conductivity of AEMs trailed that of PEMs by a significant factor. Nafion 117,[10] as the benchmark PEM, has a proton conductivity of 78 mS cm^{-1},[11] whereas anion conductivities of AEMs used to lie in the range of 5−20 mS cm^{-1}.[12] However, over the last 10 years, conductivities of AEMs have seen significant improvement, with values reported recently in the range from 50 to 200 mS cm^{-1}.[13−15] As a matter of fact, over the last 10 years, the number of publications on polyaromatic AEMs, including HMT-PMBI and HMT-PMPI, has increased significantly in comparison to the number of publications on polyolefin and perfluorinated PEMs, which had stagnating publication numbers.[16]

Over the past years, materials chemists have tested strategies in chemical design and synthesis to overcome the issue of the poor chemical stability of AEMs.[17] The most common cationic moieties employed are phosphonium-,[18] sulfonium-,[19] pyridinium-,[20] ammonium-,[21] and imidazolium-based cations, among which benzimidazolium is the most promising in terms of stability and synthetic route.[13,22,23] In a charged benzimidazole ring, the nitrogen cation stability is provided by steric protection via methyl groups.[24]

This work focuses on a sterically C2-protected poly-(benzimidazole) material, called poly-(hexamethyl-*p*-terphenylbenzimidazolium) or in short HMT-PMBI, that was developed by Holdcroft and co-workers.[25] This compound is hydroxide-stable, methanol-soluble, and water-insoluble, which renders it highly suitable for uses in fuel cells and electrolyzers.[8,25] It exhibits unprecedented hydroxide stability and ion conductivity from 25 to 80 °C and concentrations from 1 to 6 M NaOH, and it was synthesized with varying degree of methylation (dm), as reported in ref 25. In that article, only 6% chemical degradation was reported when the HMT-PMBI membrane was exposed to 2 M NaOH at 80 °C for 7 days.

Despite its promising attributes, to the best of our knowledge, only one density functional theory (DFT) work has been performed on the HMT-PMBI material,[8] but no comprehensive computational exploration of its molecular conformation and electronic structure has been reported so far. Because physical properties of HMT-PMBI are strongly affected by the degree of methylation, in this study, we consider the degree of methylation as the main parameter.[8,22]

Received: September 22, 2019
Accepted: December 4, 2019
Published: January 10, 2020

© 2020 American Chemical Society

DOI: 10.1021/acsomega.9b03116
ACS Omega 2020, 5, 1472−1478

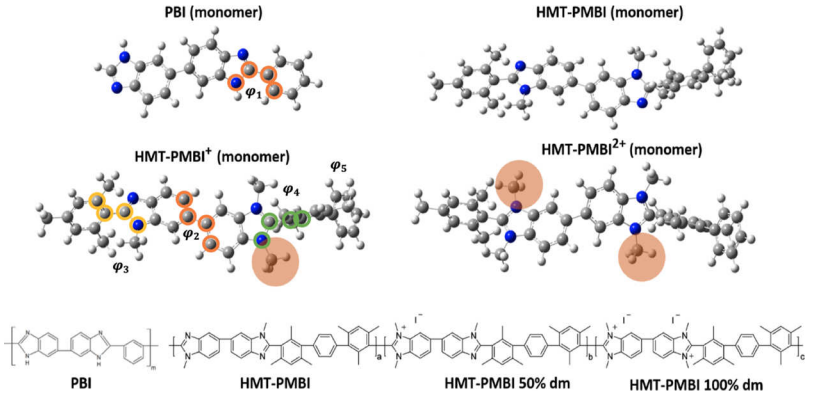

Figure 1. Chemical structure of the repeating unit of PBI, HMT-PMBI, HMT-PMBI^{+}, and HMT-PMBI^{2+}.

Table 1. Comparison of Torsional Angles between Phenyl, Benzimidazole, and Mesitylene Groups for Various Repeating Unit Study Systems[a]

	φ_{phenyl_benz} (φ_1)	φ_{benz_benz} (φ_2)	φ_{mes_benz} (φ_3)	φ_{benz_mes} (φ_4)	φ_{mes_phenyl} ($\varphi 5$)
PBI	7.60	38.9			
HMT-PMBI		37.9	103.7	106.6	83.2
HMT-PMBI^{+}		35.9	103.3	86.3	89.8
HMT-PMBI^{2+}		40.4	97.8	81.9	92.3

[a]Torsional angles are shown in Figure 1).

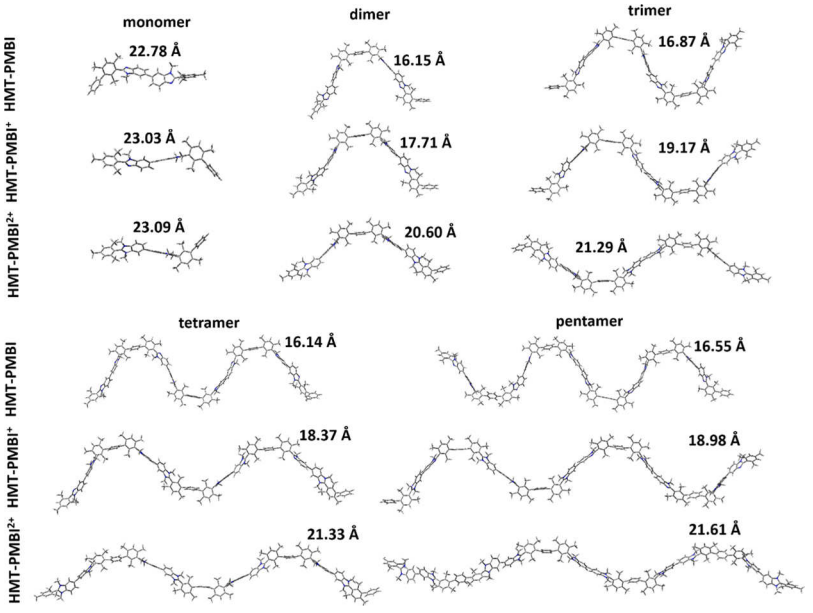

Figure 2. Effect of charge on the conformations of various studied systems in the gas phase. Numbers represent the normalized end-to-end distance values.

The primary objective of this study is to understand the effect of the degree of methylation on molecular conformation, electronic structure, and optical properties of HMT-PMBI.

2. RESULTS AND DISCUSSION

Optimized structures of the repeating unit of PBI, HMT-PMBI, HMT-PMBI^{+}, and HMT-PMBI^{2+} obtained using the B3LYP functional under vacuum conditions are shown in Figure 1. For PBI, the phenyl ring and the two adjoining benzimidazole rings are in-plane. The torsional angle between two adjoining benzimidazole rings was found to be 39°, and the one between phenyl and benzimidazole rings was 7.6°, as also shown in Table 1. For the HMT-PMBI repeating unit, however, because of the steric interaction between the mesitylene ring and benzimidazole group, a torsional angle of about 104° is formed. Considering the fully methylated HMT-PMBI repeating unit, the angle between the adjacent benzimidazole and mesitylene planes is about 82°, and it is 40° between two consecutive benzimidazole groups. By increasing the degree of methylation, the angle between the adjacent mesitylene and benzimidazole planes decreases from 107° to about 82°, as shown in Table 1. The reason for this change is the additional methyl group in the benzimidazole unit, which provides steric protection to the cationic imidazole rings.

DOI: 10.1021/acsomega.9b03116
ACS Omega 2020, 5, 1472−1478

Figure 2 shows the optimized structures from the monomer up to the pentamer of the neutral and the charged HMT-PMBI polymers along with their end-to-end distances, which are normalized to the number of repeating units. As can be seen, results reveal a trend in the chain conformation of HMT-PMBI as a function of the degree of methylation. As the charge increases, the normalized end-to-end distance becomes larger from around 16 Å for HMT-PMBI to around 19 Å for HMT-PMBI^{+} and to around 21 Å for HMT-PMBI^{2+}. The observed chain stretching is caused by the electrostatic repulsion along the backbone. Both the gas phase and solvent studies are relevant in real systems as the hydration level is not uniform across the membrane, for example, it is possible to have our membrane in the fully hydrated condition or in the high temperature/vapor phase. Hence, we investigated the solvent effects by optimizing the tetramer structures in the presence of implicit water using the polarizable continuum model (PCM).[26,27] As expected, the charge screening provided by the solvent suppresses the electrostatic repulsion among charged backbone units, rendering the normalized end-to-end distance almost unchanged from the one obtained for the corresponding neutral polymer. The DFT-optimized structure of the 100% dm HMT-PMBI trimer in the gas phase calculated in the work of Schibli[28] shows that the angle between the adjacent mesitylene and benzimidazole groups and two adjacent benzimidazole rings is 77 and 47°, respectively, which is consistent with our findings.

Figure 3 shows the electrostatic potential energy map. On neutral HMT-PMBI, negative charge is accumulated on the

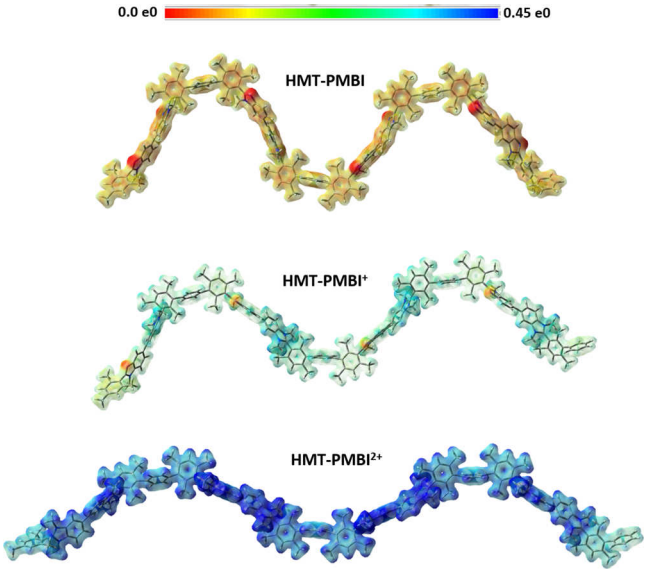

Figure 3. Electrostatic potential energy map of the tetramer of HMT-PMBIs.

nitrogen atoms of the benzimidazole ring, indicated in red. As the degree of methylation increases, more positive charge is distributed on benzimidazole groups of the backbone, as shown in darker blue for HMT-PMBI^{+} and HMT-PMBI^{2+}. This is in agreement with the observation of stretching and change in the persistence length value because of electrostatic repulsion.[29,30]

In Figure 4, the highest occupied molecular orbital (HOMO), lowest unoccupied molecular orbital (LUMO), and E_{gap}, obtained with the B3LYP functional, are plotted as functions of the oligomer length for the various degrees of methylation. As the length of the oligomer increases, the structure becomes more stabilized and HOMO, LUMO, and E_{gap} converge to specific values corresponding to the infinite (polymer) structure. For instance, for HMT-PMBI^{+}, the HOMO, LUMO, and band gap energy levels are −9.0, −6.5, and 2.5 eV, respectively. It should be noted that for charged oligomers, the drop in the energy levels from the monomer to the trimer is significantly larger (over 20 times larger) than that of the neutral HMT-PMBI and PBI oligomers. Moreover, the increasing degree of methylation causes a decrease in HOMO and LUMO energy levels and in the band gap of HMT-PMBI. The band gap for HMT-PMBI^{+} and HMT-PMBI^{2+} is decreased by approximately 2.0 and 3.0 eV relative to neutral HMT-PMBI, respectively. The values of HOMO, LUMO, and E_{gap} are shown in Table 2. HOMO and LUMO levels of neutral HMT-PMBI lie slightly above those of PBI, as shown in Figure 4; consequently, the band gap of PBI is lower than that of HMT-PMBI by about 0.5 eV. In general, the relatively large values of E_{gap} imply that HMT-PMBI-based polymers have insulator properties, as is known from experimental characterization.[31]

Figure 5 shows the molecular orbitals for the repeating units of the studied systems in the gas phase and in the presence of implicit water. Evidently, introducing an electron diminishing group onto the polymer backbone, that is, a methyl group, has significant influence on the HOMO and LUMO energy levels. For the PBI repeating unit, the HOMO level is delocalized along the backbone, indicating a strong electronic coupling between the subunits. On the neutral HMT-PMBI repeating unit, both in the absence and the presence of solvent, the HOMO level is predominantly localized on the benzimidazole groups and the contributions from phenyl and mesitylene rings are almost negligible. Weaker electronic coupling is expected in this case because of the relatively large torsional angles between these groups. On 75% dm HMT-PMBI, the HOMO level is further localized with a negligible contribution from the charged nitrogen of the benzimidazole unit. This trend is more significant on fully methylated HMT-PMBI, where the HOMO is strongly localized on the phenyl unit. In the presence of implicit water, however, the HOMO is more delocalized because of the charge screening effect exerted by the solvent. As also shown in Figure 5, the electron densities of the LUMO of PBI and HMT-PMBI are rather delocalized, while those for HMT-PMBI^{+} and HMT-PMBI^{2+} are more localized on the charged units both in the gas phase and in the presence of implicit water.

The changes in the polymer charge because of the varying degree of methylation and consequent conformational changes along the backbone have an impact on the UV−vis absorption spectra as could be measured in photoluminescence experiments.[32] We used time-dependent DFT (TD-DFT) to investigate the excited states of the repeating units of neutral, partially, and fully methylated HMT-PMBI. As shown in Figure 6, the spectrum of HMT-PMBI^{+} exhibits two peaks associated with the two separate electronic transitions in its corresponding structure. The spectra for the HMT-PMBI^{+} and HMT-PMBI^{2+} structures are shifted to longer wavelengths relative to the HMT-PMBI structure, which is not surprising because as discussed, the band gap decreases for the charged polymers.

Peaks become broader as the degree of methylation increases. The spectrum for HMT-PMBI is centered near

DOI: 10.1021/acsomega.9b03116
ACS Omega 2020, 5, 1472−1478

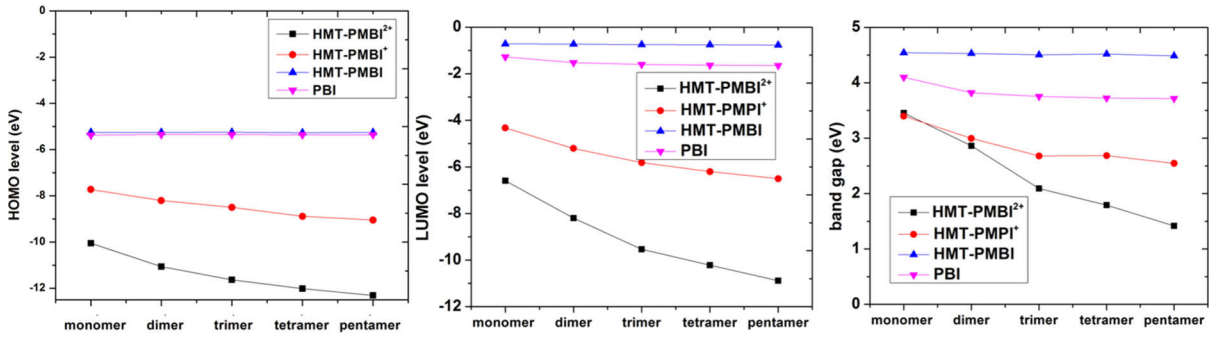

Figure 4. HOMO, LUMO, and band gap of the studied polybenzimidazole-based ionenes.

Table 2. Comparison of HOMO, LUMO, and Band Gap Data of Different Oligomers of PBI and HMT-PMBIs Using the B3LYP Functional

	PBI			HMT-PMBI			HMT-PMBI$^+$			HMT-PMBI^{2+}		
material functional	HOMO	LUMO	E_{gap}	HOMO	LUMO	E_{gap}	HOMO	LUMO	E_{gap}	HOMO	LUMO	E_{gap}
monomer	−5.38	−1.28	4.10	−5.26	−0.72	4.54	−7.72	−4.33	3.40	−10.05	−6.60	3.45
dimer	−5.35	−1.52	3.82	−5.26	−0.73	4.53	−8.21	−5.21	2.99	−11.06	−8.20	2.86
trimer	−5.36	−1.60	3.75	−5.25	−0.75	4.50	−8.50	−5.82	2.68	−11.63	−9.54	2.09
tetramer	−5.36	−1.64	3.72	−5.27	−0.75	4.52	−8.89	−6.20	2.68	−12.01	−10.22	1.79
pentamer	−5.36	−1.65	3.71	−5.26	−0.77	4.49	−9.05	−6.50	2.55	−12.31	−10.89	1.42

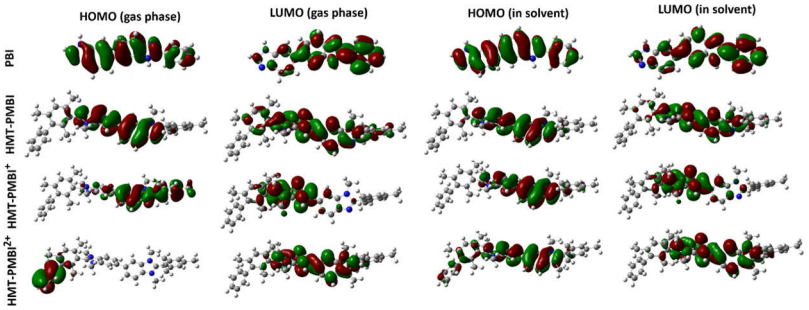

Figure 5. HOMO and LUMO of the studied systems in the gas phase and in the presence of water solvent.

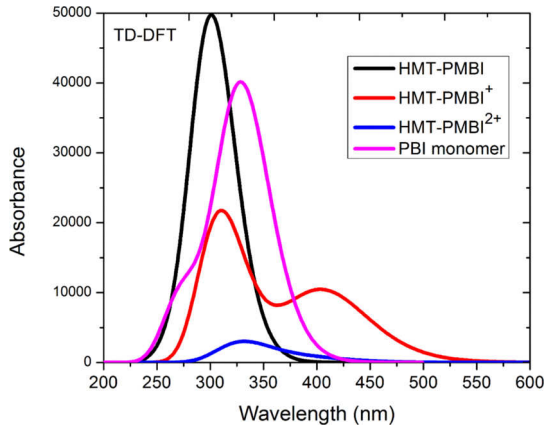

Figure 6. Absorption spectra of the various repeating units of polybenzimidazole-based ionenes using TD-DFT.

300 nm; for HMT-PMBI$^+$, the broader peak is at around 410 nm, while the narrower one is at 310 nm, and for HMT-PMBI^{2+}, the broad peak is at 330 nm. In addition, in Figure 6, the spectrum of the PBI repeating unit is shown with a peak centered at 330 nm and a shoulder at 275 nm. This agrees well with experimental results in ref 32, where two distinct peaks were reported by the authors in the absorption spectrum of PBI, one at 284 nm (4.36 eV) and another one at 360 nm (3.44 eV), which corresponded to the $\pi \rightarrow \pi^*$ transition in their work.[32]

In Table 3, we report the HOMO, LUMO, and E_{gap} values for the tetramer of PBI and HMT-PMBIs with various degrees of methylations obtained with different DFT functionals.

As shown in Figure 7, the choice of the DFT functional results in similar trends for all systems; Grimme's functional including dispersion, B97D, as well as PBE and TPSS functionals, which are at the generalized gradient approximation (GGA) and meta-GGA level, respectively, predict higher values for the HOMO compared to the hybrid functionals, namely, O3LYP, B3LYP, PBE1, and wB97XD. The HOMO level predicted by wB97XD is significantly lower than that for the other functionals. Likewise, the LUMO predicted by B97D, PBE, and TPSS is smaller than those predicted by hybrid functionals, while the LUMO obtained with the wB97XD functional is significantly larger than that for other functionals. Therefore, wB97XD gives the largest value of E_{gap} for all systems by a difference in the range between 3 and 5 eV. E_{gap} calculated by PBE1 is larger than that found with B3LYP by about 0.3−0.4 eV and that for B3LYP is larger than the value for O3LYP by about 0.4−0.5 eV. In turn, E_{gap} values predicted by PBE and TPSS are smaller than that obtained with B3LYP by 1.0−1.5 eV. B97D, on the other hand, predicts

DOI: 10.1021/acsomega.9b03116
ACS Omega 2020, 5, 1472−1478

Table 3. Comparison of HOMO, LUMO, and Band Gap Data of the Tetramer of PBI and HMT-PMBIs Using Various Functionals

	PBI			HMT-PMBI			HMT-PMBI$^+$			HMT-PMBI^{2+}		
material functional	HOMO	LUMO	E_{gap}	HOMO	LUMO	E_{gap}	HOMO	LUMO	E_{gap}	HOMO	LUMO	E_{gap}
B97D	−4.66	−2.21	2.45	−4.50	−1.48	3.02	−7.95	−6.81	1.14	−11.17	−10.78	0.39
PBE	−4.77	−2.31	2.45	−4.61	−1.53	3.08	−8.10	−6.90	1.19	−11.27	−10.89	0.39
TPSS	−4.75	−2.20	2.55	−4.60	−1.40	3.20	−8.12	−6.78	1.34	−11.27	−10.76	0.51
O3LYP	−5.08	−1.81	3.27	−4.96	−0.84	4.11	−8.58	−6.39	2.19	−11.66	−10.41	1.25
B3LYP	−5.36	−1.64	3.72	−5.27	−0.75	4.52	−8.88	−6.20	2.68	−12.01	−10.22	1.79
PBE1	−5.62	−1.55	4.07	−5.52	−0.69	4.82	−9.11	−6.11	3.00	−12.33	−10.12	2.22
wB97XD	−7.23	−0.12	7.11	−7.17	1.01	8.17	−10.81	−4.47	6.34	−14.06	−8.44	5.62

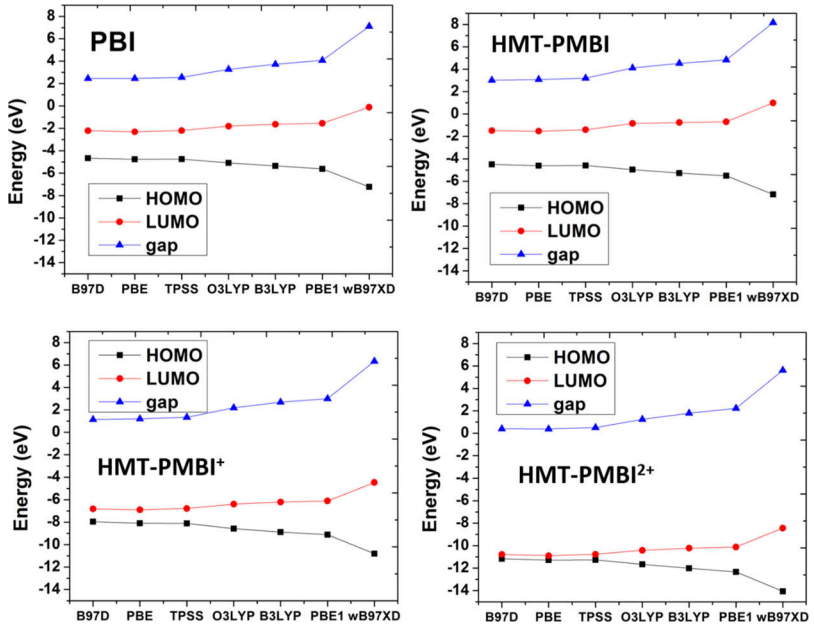

Figure 7. Effect of different density functionals on the HOMO, LUMO, and band gap of PBI and HMT-PMBI tetramers.

similar values to the PBE functional with a difference smaller than 0.05 eV. Similar calculations for π-conjugated polymers reported in ref 33 suggest that B3LYP is in better agreement with experimental values.[33] However, experimental characterization employing, for instance, cyclic voltammetry and UV−visible spectra is needed to determine, which functional provides the most accurate prediction of ionene properties.

3. CONCLUSIONS

This work focused on the conformational properties of HMT-PMBI oligomers. We demonstrated that the ionic charge distribution, electronic structure, and optical properties of single ionene moieties can be calculated well with DFT. Results indicate an increase in the electrostatic repulsion of ionene moieties in the gas phase with the increasing degree of methylation, leading to a stretching of the chains. The presence of water, however, suppresses the electrostatic repulsion among ionene charges. We calculated the HOMO, LUMO, and electronic band gap of various HMT-PMBIs. More positive charge on the backbone leads to a decrease, by about 2.0 and 3.0 eV, of the band gaps of HMT-PMBI$^+$ and HMT-PMBI^{2+} relative to that for the neutral polymer, respectively. Consistently, in the TD-DFT study, it was seen that the absorption spectrum of the methylated repeating units is red-shifted relative to the neutral ones.

Studying the single chain behavior is a prerequisite for studying self-organization in concentrated solutions of polybenzimidazole ionenes. Studies performed and reported here reveal important trends in this regard, and they could thus form the basis for further modeling and simulation of ionene self-aggregation, network formation, ion and solvent transport, and the development of a statistical model of fracture formation in ionene-based membranes. Insights on the conformational properties of ionenes with varying degree of methylation is important for better understanding the charge transport behavior in ionene solution. We hope that this study would prompt further fundamental investigations on conformational properties of benzimidazolium compounds.

4. COMPUTATIONAL DETAILS

Calculations in this work have been performed with Gaussian 16.[34] We performed DFT calculations from the monomer to the pentamer of HMT-PMBI. The HMT-PMBI repeating unit with 50% degree of methylation is electroneutral, while 75 and 100% degrees of methylation correspond to the charge +1 and +2, respectively.[25] We calculated the electronic band gap, E_{gap}, which is defined as the minimal energy difference between HOMO and LUMO levels.

All structures were fully optimized to find the ground state energy. The condition for attaining the ground state is satisfied when the gradient of the total energy with respect to the

DOI: 10.1021/acsomega.9b03116
ACS Omega 2020, 5, 1472−1478

nuclear coordinates is zero. The convergence criterion for the calculation is as follows:[34] the maximum component of the total force must be below a cutoff value of 0.00045 N; the root-mean-square of the force below 0.0003 N; the calculated displacement for the next step below a cutoff value of 0.0018 Å; and the root-mean-square of the displacement for the next step below 0.0012 Å. We employed the 6-31G(d) basis set.

We tested various functionals for calculating the HOMO, LUMO, and E_{gap}, including B97D, Grimme's functional with the dispersion correction;[35] the PBE functional, which is at the GGA level;[36] the TPSS functional, which is a nonempirical meta-GGA;[37] O3LYP[29] and B3LYP[38] hybrid functionals, which are very similar but have slightly different mixing coefficients; PBE1, which is also a hybrid exchange−correlation functional based on the GGA PBE;[39] and wB97XD,[40] which is known as a range-separated functional that includes Grimme's D2 dispersion model[35] to capture both short-range interactions and long-range corrections. Our main motive for testing these seven DFT functionals was to explore how well they can describe the electronic properties of the ionene system in comparison to the B3LYP functional, which is the only functional used to date for this system.[28]

Using TD-DFT,[41] we extracted excited-state data and generated UV−vis absorption spectra. Solvent effects were investigated by optimizing the tetramer structures in the presence of implicit water using the PCM.[26,27] GaussView 6.0 visualization software was used to generate the input structures and display the output geometries and orbitals.[42]

AUTHOR INFORMATION

Corresponding Author

*E-mail: meslamib@sfu.ca.

ORCID

Mohammad Javad Eslamibidgoli: 0000-0002-5057-2993

Author Contributions

§M.M. and M.J.E. had equal contributions in this manuscript.

Notes

The authors declare no competing financial interest.

ACKNOWLEDGMENTS

This research was conducted as part of the Engineered Nickel Catalysts for Electrochemical Clean Energy project administered from Queen's University and supported by grant no. RGPNM 477963-2015 under the Natural Sciences and Engineering Research Council of Canada (NSERC) Discovery Frontiers Program. This research was enabled in part by support provided by ComputeCanada Calcul Canada (www.computecanada.ca).

REFERENCES

(1) Varcoe, J. R.; Slade, R. C. T. Prospects for alkaline anion-exchange membranes in low temperature fuel cells. *Fuel Cells* **2005**, *5*, 187−200.

(2) Lufrano, F.; Gatto, I.; Staiti, P.; Antonucci, V.; Passalacqua, E. Sulfonated poly-sulfone ionomer membranes for fuel cells. *Solid State Ionics* **2001**, *145*, 47−51.

(3) Dekel, D. R. Review of cell performance in anion exchange membrane fuel cells. *J. Power Sources* **2018**, *375*, 158−169.

(4) Marini, S.; Salvi, P.; Nelli, P.; Pesenti, R.; Villa, M.; Berrettoni, M.; Zangari, G.; Kiros, Y. Advanced alkaline water electrolysis. *Electrochim. Acta* **2012**, *82*, 384−391.

(5) Lin, K.; Chen, Q.; Gerhardt, M. R.; Tong, L.; Kim, S. B.; Eisenach, L.; Valle, A. W.; Hardee, D.; Gordon, R. G.; Aziz, M. J.; Marshak, M. P. Alkaline quinone flow battery. *Science* **2015**, *349*, 1529−1532.

(6) Liao, Q.; Zhang, J.; Li, J.; Ye, D.; Zhu, X.; Zheng, J.; Zhang, B. Electricity generation and COD removal of microbial fuel cells (MFCs) operated with alkaline substrates. *Int. J. Hydrogen Energy* **2014**, *39*, 19349−19354.

(7) An, L.; Zhao, T. S.; Shen, S. Y.; Wu, Q. X.; Chen, R. Alkaline direct oxidation fuel cell with non-platinum catalysts capable of converting glucose to electricity at high power output. *J. Power Sources* **2011**, *196*, 186−190.

(8) Schibli, E. M.; Wright, A. G.; Holdcroft, S.; Frisken, B. J. Morphology of Anion-Conducting Ionenes Investigated by X-ray Scattering and Simulation. *J. Phys. Chem. B* **2018**, *122*, 1730−1737.

(9) Weber, A. Z.; Newman, J. Transport in Polymer-Electrolyte Membranes. *J. Electrochem. Soc.* **2003**, *150*, A1008−A1015.

(10) Zawodzinski, T. A.; Derouin, C.; Radzinski, S.; Sherman, R. J.; Smith, V. T.; Springer, T. E.; Gottesfeld, S. Water uptake by and transport through Nafion 117 membranes. *J. Electrochem. Soc.* **1993**, *140*, 1041−1047.

(11) Sone, Y.; Ekdunge, P.; Simonsson, D. Proton conductivity of Nafion 117 as measured by a four-electrode AC impedance method. *J. Electrochem. Soc.* **1996**, *143*, 1254−1259.

(12) Merle, G.; Wessling, M.; Nijmeijer, K. Anion exchange membranes for alkaline fuel cells: A review. *J. Membr. Sci.* **2011**, *377*, 1−35.

(13) Hagesteijn, K. F. L.; Jiang, S.; Ladewig, B. P. A review of the synthesis and characterization of anion exchange membranes. *J. Matter. Sci.* **2018**, *53*, 11131−11150.

(14) Zheng, Y.; Ash, U.; Pandey, R. P.; Ozioko, A. G.; Ponce-González, J.; Handl, M.; Weissbach, T.; Varcoe, J. R.; Holdcroft, S.; Liberatore, M. W.; Hiesgen, R.; Dekel, D. R. Water uptake study of anion exchange membranes. *Macromolecules* **2018**, *51*, 3264−3278.

(15) Li, Z.; He, X.; Jiang, Z.; Yin, Y.; Zhang, B.; He, G.; Tong, Z.; Wu, H.; Jiao, K. Enhancing hydroxide conductivity and stability of anion exchange membrane by blending quaternary ammonium functionalized polymers. *Electrochim. Acta* **2017**, *240*, 486−494.

(16) Park, E. J.; Kim, Y. S. Quaternized aryl ether-free polyaromatics for alkaline membrane fuel cells: synthesis, properties, and performance−a topical review. *J. Matter. Chem. A* **2018**, *6*, 15456−15477.

(17) Neagu, V.; Bunia, I.; Plesca, I. Ionic Polymers VI. Chemical Stability of Strong Base Anion Exchangers in Aggressive Media. *Polym. Degrad. Stab.* **2000**, *70*, 463−468.

(18) Noonan, K. J. T.; Hugar, K. M.; Kostalik, H. A.; Lobkovsky, E. B.; Abruña, H. D.; Coates, G. W. Phosphonium-functionalized polyethylene: a new class of base-stable alkaline anion exchange membranes. *J. Am. Chem. Soc.* **2012**, *134*, 18161−18164.

(19) Zhang, B.; Gu, S.; Wang, J.; Liu, Y.; Herring, A. M.; Yan, Y. Tertiary sulfonium as a cationic functional group for hydroxide exchange membranes. *RSC Adv.* **2012**, *2*, 12683−12685.

(20) Huang, A.; Xia, C.; Xiao, C.; Zhuang, L. Composite anion exchange membrane for alkaline direct methanol fuel cell: structural and electrochemical characterization. *J. Appl. Polym. Sci.* **2006**, *100*, 2248−2251.

(21) Wang, J.; Wang, J.; Zhang, S. Synthesis and characterization of cross-linked poly (arylene ether ketone) containing pendant quaternary ammonium groups for anion-exchange membranes. *J. Membr. Sci.* **2012**, *415−416*, 205−212.

(22) Wright, A. G.; Holdcroft, S. Hydroxide-Stable Ionenes. *ACS Macro Lett.* **2014**, *3*, 444−447.

(23) Xu, T. Ion exchange membranes: state of their development and perspective. *J. Membr. Sci.* **2005**, *263*, 1−29.

(24) Wright, A. G.; Weissbach, T.; Holdcroft, S. Poly(Phenylene) and m-Terphenyl as Powerful Protecting Groups for the Preparation of Stable Organic Hydroxides. *Angew. Chem., Int. Ed.* **2016**, *55*, 4818−4821.

(25) Wright, A. G.; Fan, J.; Britton, B.; Weissbach, T.; Lee, H.-F.; Kitching, E. A.; Peckham, T. J.; Holdcroft, S. Hexamethyl-p-Terphenyl Poly(Benzimidazolium): a Universal Hydroxide-Conduct-

DOI: 10.1021/acsomega.9b03116
ACS Omega 2020, 5, 1472−1478

ing Polymer for Energy Conversion Devices. *Energy Environ. Sci.* **2016**, *9*, 2130−2142.
(26) Miertuš, S.; Scrocco, E.; Tomasi, J. Electrostatic Interaction of a Solute with a Continuum. A Direct Utilization of ab initio Molecular Potentials for the Prevision of Solvent Effects. *Chem. Phys.* **1981**, *55*, 117−129.
(27) Pascual-Ahuir, J. L.; Silla, E.; Tuñon, I. GEPOL: An improved description of molecular-surfaces. 3. A new algorithm for the computation of a solvent-excluding surface. *J. Comput. Chem.* **1994**, *15*, 1127−1138.
(28) Schibli, E. M. Analysis of novel ionenes via X-ray and neutron scattering. M.Sc. Thesis, Simon Fraser University, 2016.
(29) Cohen, A. J.; Handy, N. C. Dynamic correlation. *Mol. Phys.* **2001**, *99*, 607−615.
(30) Tegenfeldt, J. O.; Prinz, C.; Cao, H.; Chou, S.; Reisner, W. W.; Riehn, R.; Wang, Y. M.; Cox, E. C.; Sturm, J. C.; Silberzan, P.; Austin, R. H. The dynamics of genomic-length DNA molecules in 100-nm channels. *Proc. Natl. Acad. Sci. U.S.A.* **2004**, *101*, 10979−10983.
(31) Arun, M.-K.; Chandrasekaran, A.; Kim, C.; Huan, T. D.; Pilania, G.; Botu, V.; Ramprasad, R. Scoping the polymer genome: A roadmap for rational polymer dielectrics design and beyond. *Mater. Today* **2018**, *21*, 785−796.
(32) Prabunathan, P.; Hariharan, A.; Alagar, M. Photoluminescence and Electrochemical Behaviors of Polybenzimidazole-Grafted Carbon Nanotubes. *Polym-plast. Technol.* **2016**, *55*, 542−551.
(33) Boschetto, G.; Xue, H.-T.; Dziedzic, J.; Krompiec, M.; Skylaris, C.-K. Effect of polymerization statistics on the electronic properties of copolymers for organic photovoltaics. *J. Phys. Chem. C* **2017**, *121*, 2529−2538.
(34) Frisch, M. J.; Trucks, G. W.; Schlegel, H. B.; Scuseria, G. E.; Robb, M. A.; Cheeseman, J. R.; Scalmani, G.; Barone, V.; Petersson, G. A.; Nakatsuji, H.; Li, X.; Caricato, M.; Marenich, A. V.; Bloino, J.; Janesko, B. G.; Gomperts, R.; Mennucci, B.; Hratchian, H. P.; Ortiz, J. V.; Izmaylov, A. F.; Sonnenberg, J. L.; Williams-Young, D.; Ding, F.; Lipparini, F.; Egidi, F.; Goings, J.; Peng, B.; Petrone, A.; Henderson, T.; Ranasinghe, D.; Zakrzewski, V. G.; Gao, J.; Rega, N.; Zheng, G.; Liang, W.; Hada, M.; Ehara, M.; Toyota, K.; Fukuda, R.; Hasegawa, J.; Ishida, M.; Nakajima, T.; Honda, Y.; Kitao, O.; Nakai, H.; Vreven, T.; Throssell, K.; Montgomery, J. A., Jr.; Peralta, J. E.; Ogliaro, F.; Bearpark, M. J.; Heyd, J. J.; Brothers, E. N.; Kudin, K. N.; Staroverov, V. N.; Keith, T. A.; Kobayashi, R.; Normand, J.; Raghavachari, K.; Rendell, A. P.; Burant, J. C.; Iyengar, S. S.; Tomasi, J.; Cossi, M.; Millam, J. M.; Klene, M.; Adamo, C.; Cammi, R.; Ochterski, J. W.; Martin, R. L.; Morokuma, K.; Farkas, O.; Foresman, J. B.; Fox, D. J. *Gaussian 09*, Revision D. 01, Gaussian, Gaussian 16, Revision B.01; Gaussian, Inc.: Wallingford CT, 2016.
(35) Grimme, S. Semiempirical GGA-type density functional constructed with a long-range dispersion correction. *J. Comput. Chem.* **2006**, *27*, 1787−1799.
(36) Perdew, J. P.; Burke, K.; Ernzerhof, M. Generalized gradient approximation made simple. *Phys. Rev. Lett.* **1996**, *77*, 3865−3868.
(37) Tao, J.; Perdew, J. P.; Staroverov, V. N.; Scuseria, G. E. Climbing the density functional ladder: Nonempirical meta-generalized gradient approximation designed for molecules and solids. *Phys. Rev. Lett.* **2003**, *91*, 146401.
(38) Becke, A. D. Density-functional thermochemistry. III. The role of exact exchange. *J. Chem. Phys.* **1993**, *98*, 5648−5652.
(39) Adamo, C.; Barone, V. Toward reliable density functional methods without adjustable parameters: The PBE0 model. *J. Chem. Phys.* **1999**, *110*, 6158−6170.
(40) Chai, J.-D.; Head-Gordon, M. Long-range corrected hybrid density functionals with damped atom-atom dispersion corrections. *Phys. Chem. Chem. Phys.* **2008**, *10*, 6615−6620.
(41) Bauernschmitt, R.; Ahlrichs, R. Treatment of electronic excitations within the adiabatic approximation of time dependent density functional theory. *Chem. Phys. Lett.* **1996**, *256*, 454.
(42) Dennington, R.; Keith, T. A.; Millam, J. M. *GaussView*, version 6; Semichem Inc.: Shawnee Mission, KS, 2016.

DOI: 10.1021/acsomega.9b03116
ACS Omega 2020, 5, 1472−1478